Department of Precision and Microsystems Engineering

# On-chip acoustic trapping of sub-micron objects with surface acoustic wave devices

Jichao Shan

Report no : 2022.051
Coach : Dr. Sabina Caneva; Dr. Andres Hunt
Specialisation : MNE
Type of report : Master Thesis
Date : 24 August 2022

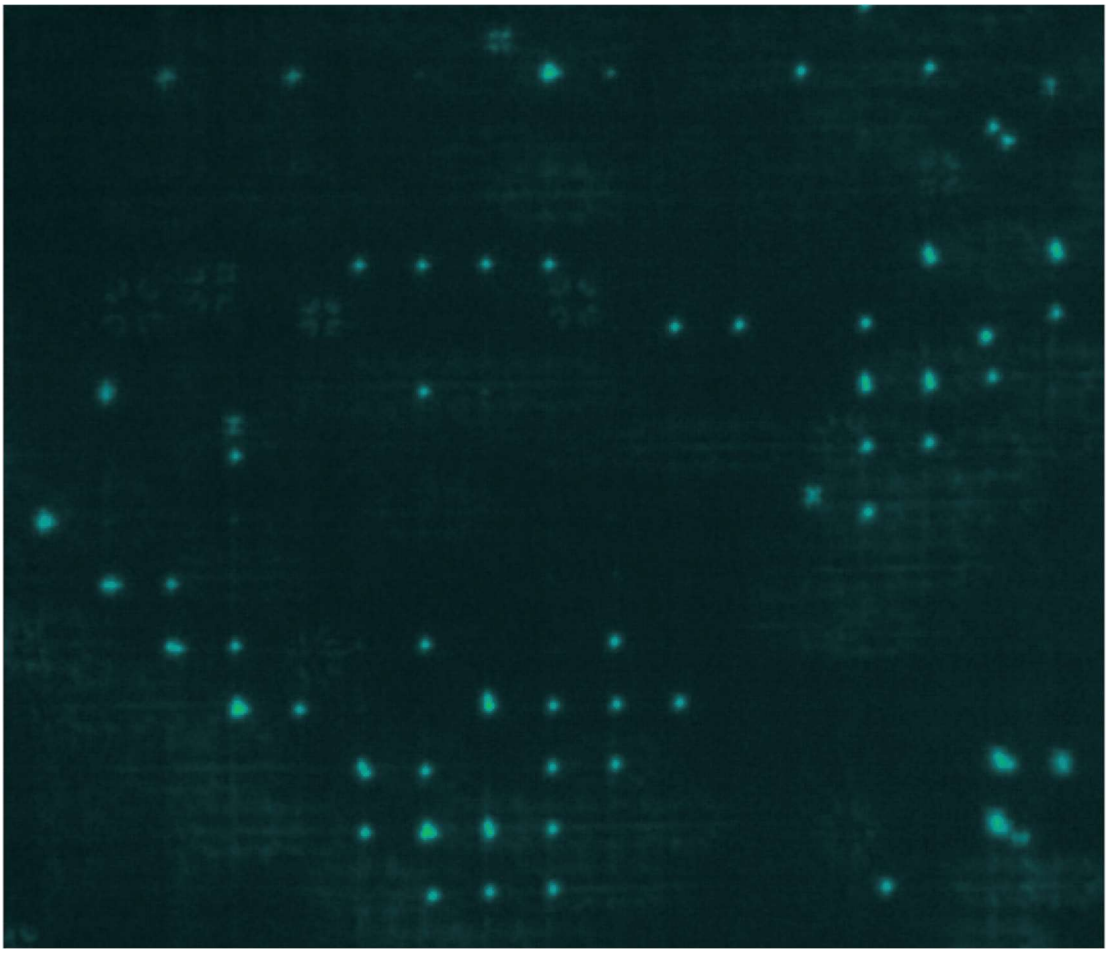

**MSc thesis in Mechanical Engineering**

# On-chip acoustic trapping of sub-micron objects with surface acoustic wave devices

Jichao Shan

31 August 2022

A thesis submitted to the Delft University of Technology in partial fulfillment of the requirements for the degree of Master of Science in Mechanical Engineering

| | | |
|---|---|---|
| Student number: | 5253128 | |
| Project duration: | November, 2021 – August, 2022 | |
| Thesis committee: | Dr. S. Caneva, | TU Delft, Senior supervisor, Chair, DMN, MNE, PME, 3ME |
| | Dr. A. Hunt, | TU Delft, Supervisor, PME, MNE, 3ME |
| | Dr. S. Iskander-Rizk, | TU Delft, MOOM, PME, 3ME |
| | Dr. M.K. Ghatkesar, | TU Delft, MNE, PME, 3ME |

# Abstract

Proteins play a key role in many biological processes and are thus useful indicators of health and disease states. Since the size of proteins is few hundred nanometers, it is necessary to explore new techniques to manipulate and 'read' them. This thesis aims to identify and build a platform that enables sub-micron bead manipulation, which will be used to actively deliver the biomolecules attached to the beads to the single-molecule sensor. During this process, accurate positioning, speed control, and multiplexing of the beads need to be solved to give high-resolution and high-throughput sequencing capabilities. We identify surface acoustics wave (SAW) devices as powerful tools to achieve both beads transport and massively parallel manipulation. Our hypothesis is that we can increase the efficiency and precision of bead capture and manipulation by using SAW devices combined with a microcavity layer. In this master thesis, we fabricate the SAW device with an average 2 $\mu m$ thick film, and there are cavity arrays on the film. In addition, we investigate the performance of trapping sub-micron objects during the actuation. Further more, we discuss few challenges found through the experiments and provide possible solutions for them. At last, this thesis is concluded by discussing the work been done and providing suggestions for future experiments.

# Acknowledgements

I've worked hard and put in a lot of efforts over the past few months. I'm happy that everything worked out as expected in the end. Now I am writing the last page of my master thesis, and I would like to thank the few people who accompanied me along the journey. First I'd like to say thank you to Sabina Caneva, my supervisor, for supports through the entire year, especially when I am having a hard time on the project, Andres Hunt for the wise suggestions and encourage during the meetings we had, XiLiang Yang used her own time to fabricate SAW device for me, Dong Hoon Shin for listening many challenges that I faced and provide me as much help as possible, and every staff in the lab that gave the trainings to me. Besides, I'd like to thank my mom, dad and all my friends who supported me when I needed help the most. Last but not least, I would like to say that without this support, I could not have done this wonderful work.

...

# Contents

# 1 Introduction

### 1.0.1 Proteins in health and disease

Proteins perform a number of critical biological functions as enzymes, structural proteins or hormones. For instance, insulin as a protein-based hormone regulates the level of glucose in the blood. Thus, secretion of insulin indicates a person's health state. Protein biosynthesis plays a key role in disease since changes and errors in this process, in the form of DNA mutations and hence protein misfolding, are often the underlying causes of a disease. Well known examples are Alzheimer's and Parkinson diseases, both originating from incorrect protein folding. Protein dysfunction can originate either because of mutations during the transcription (DNA to RNA) and translation (RNA to protein) processes, or because of subsequent modifications of the protein after it is synthesized i.e. post-translational modifications. [1]

Proteins are assembled from amino acids (i.e. the building blocks) using information encoded in genes. Each protein has its own unique amino acid sequence that is specified by the nucleotide sequence of the gene encoding this protein. Mutation of a single nucleotide generates a different amino acid after transcription and translation. Thus DNA sequencing can help to quickly identify mutant genes from patients. [2]

DNA sequencing is also being increasingly used to diagnose and treat rare diseases. As more and more genes are identified that cause rare genetic diseases, we anticipate that molecular diagnoses for patients becomes more mainstream. DNA sequencing allows clinicians to identify genetic diseases. In recent years, DNA/RNA sequencing technologies have also been used to screen the genome of viruses, such as the SARS-Cov-2 virus. It is therefore extremely important to be able to sequence these molecules with high accuracy in order find cures and develop effective vaccines.[3]

### 1.0.2 Single-molecule techniques

Single-molecule techniques are being developed to 'see', 'touch' and 'sense' individual biomolecules. They have already shown great promise in solving the challenges related to the nanoscale dimensions of the components and structures under investigation. In particular, nanofluidic devices enable exquisite control of the fluid environment of single molecules and real time addition and observation of new species in an experiment.[4] Single molecule

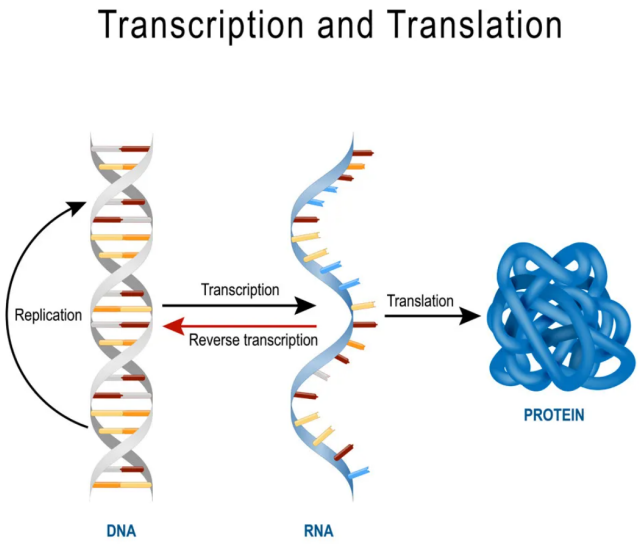


Figure 1.1: Process of protein synthesis: DNA transcription into RNA and RNA translation into a protein.

techniques can be broadly divided into methods that can image, confine or manipulate biomolecules. Optical tweezers are enable to generate geometrical centre of the focused laser beam and actuating particles towards potential energy minimum place.[5] Acoustic tweezers are versatile devices that use sound waves to spatially and temporally manipulate micron-sized objects via the interaction of the waves with solid, liquid and gases.[6] Nanopores enable to measure single-molecule electrical signal. Fluorescence image techniques are able to achieve the observation of DNA, RNA and protein activities inside living cells. These approaches have and continue to facilitate biophysics research at nanoscale.

So far all the single-molecule studies have several aspects in common. The methods can only sequence a single or few molecules at a time, which limits efficiency of sequencing single-molecules from different species in the sample that can be explored. Besides, it can be challenging to control speed of movement during sequencing of single-molecules. As a consequence, single-molecules are moving too fast to be precisely measured.

In order to better understand the links between sequence-structure-function and their role in health and disease, new methods need to be developed that can manipulate and sequence these biomolecules at single molecule level. Hence, the goal is developing a method to massively manipulate beads which have single-molecule attached to it and direct them to sequencing regions of the device. In this project, we only focus on manipulating in-plane motion of beads by using acoustic tweezer techniques. In this thesis, the motivation of the research is given first. The molecule manipulating technique is introduced in chapter 2. Then,

all kinds of techniques and tools used during fabricating the device can be found in chapter 3. In chapter 4, there is a comparison of cavities fabricated with different method. Meanwhile, results of S parameter and acoustic pressure simulations, and the microbeads motion observed with and without actuation are also discussed in chapter 4. At last, this thesis is concluded with discussing few challenges found throughout the entire experiments.

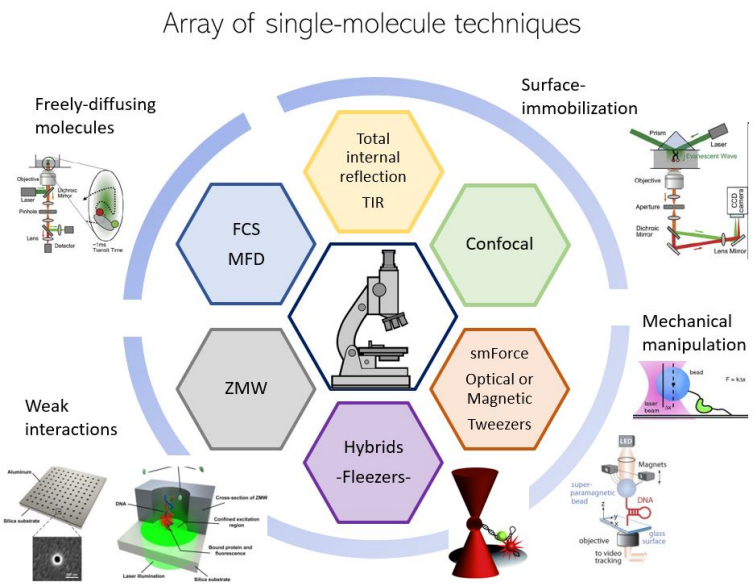


Figure 1.2: Single-molecule techniques for biomolecule imaging, confinement and/or manipulation.

# 2 Theory

## 2.1 Surface acoustic wave devices

Surface acoustic waves (SAWs) are mechanical waves that propagate on the surface of a piezoelectric material. They are generated by applying an radiofrequency signal to inter-digitated transducers (IDTs) that are patterned on the substrate.[7] An IDT consists of a set of connected metallic fingers inter-spaced with an opposite set of connected metallic fingers. Characterization of piezoelectric materials is converting electrical and mechanical energy into each other. Since this wave is localized at surface region and only extends about one wavelength into bulk direction, it has high energy density on the surface. Many single-molecule studies use this high surface energy density to transport molecules cross the surface. Figure 2.1 shows the simple principle of a standing SAW device. By applying inverse piezoelectric effect, IDTs converted electrical potential into the mechanics strain. This mechanics strain traveled cross the surface and was converted back to electrical potential which can be detected by the voltage meter. In the next section, two types of SAW devices will be described .

### 2.1.1 Standing SAW devices

A typical standing SAW device uses at least one set of metallic IDTs fabricated on the surface of a piezoelectric substrate. A standing wave is induced through interaction of two traveling acoustic wave produced by each IDTs of a set. Beads that interact with the standing acoustic wave will experience an acoustic radiation force which can be used to pattern, localize or transport the beads to desired locations on the device. Equation 2.1 shows the equation of acoustic radiation force, where $\rho$ is the acoustic pressure, v is the velocity, and $\rho^* = \rho_p/\rho_m$ and $k^* = k_p/k_m$ are density ratio and compressibility ratio between particle and the medium, respectively.[9] In a standing wave, this acoustic radiation force acts to move beads along a potential gradient towards the wave node or antinode, which depends on the respective densities and compressibilities of the particle and surrounding media.[10]

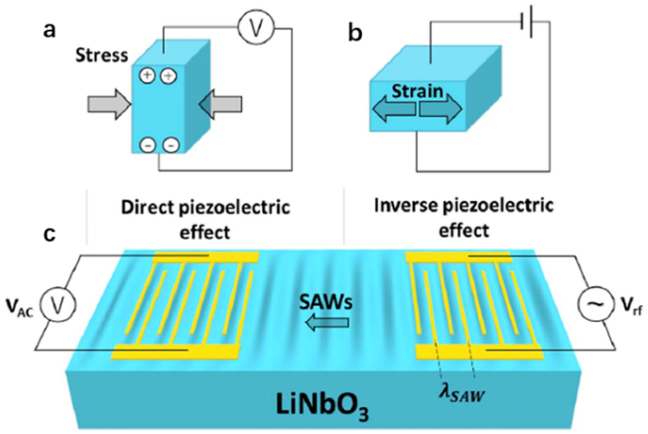


Figure 2.1: **a)** By applying direct piezoelectric effect, piezo materials generate a measurable piezoelectricity when the structures are deformed. **b)** For inverse piezoelectric effect, piezo materials would generate mechanical strain when it applied to external electrical potential. **c)** Schematic of a two port SAW device: A set of yellow metal electrodes i.e. the IDTs, are sitting on top of piezoelectric substrate e.g. $LiNbO_3$.[8]

$$F = -V\nabla[\frac{1-k^*}{4}k_m p^2 - \frac{\rho^* - 1}{2\rho^* + 1}\rho_m v^2] \tag{2.1}$$

There is a limitation in manipulating few micron objects. The efficiency of patterning micron-scale objects is also determined by ratio of $D/\lambda$, where D is object's diameter and $\lambda$ is the acoustic wavelength. In the case of $\lambda \gg D$ (Figure 2.2(a)(b)), objects aggregate at nodal locations. However, if $\lambda \approx D$ (Figure 2.2(c)(d)), objects are individually distributed at each nodal location. Since the wavelength is determined by pitch of IDTs, it can be challenging to pattern individual sub-micron objects, because IDTs with small (nanometre-scale) widths and distances are more challenging to fabricate.

### 2.1.2 Traveling SAW devices

Traveling SAW devices featuring a single IDT are often used in particle manipulation. Unlike standing wave, the particles are not moving towards node or anti-node. When a travelling SAW contacts a small volume of liquid, the liquid absorbs part of the SAW's energy and refracts it in the form of longitudinal waves. This refracted acoustic energy induces flow in the fluid, known as SAW-induced acoustic streaming and acts on any particles present in the fluid. Typically, traveling waves coupled with micro-fluidic structures are used to achieve multiplexed particles manipulation. Compared with standing-wave device, traveling-wave

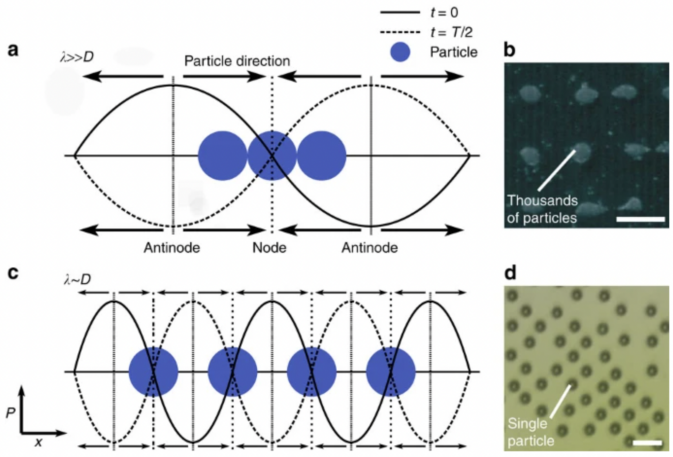


Figure 2.2: Comparison of the principle of particles patterning and aggregation. **a)** Multiple particles cohabit in a same nodal position for a relatively large wavelength. **b)** Particles aggregate at nodes in the case of a) **c)** Particles are spatially isolated while actuating with a small enough wavelength. **d)** Single particles are staying isolated.

devices can more easily be modulated in real time and are better suited for applications requiring arbitrary patterning or single object handling. [6]

## 2.2 Traveling surface acoustic wave coupled with a microcavity layer

In a previous work by Tayebi et al.[11], 300 nm beads were patterned by using acoustic-structure interactions in a SAW device containing a polymeric cavity array layer on top of the piezoelectric substrate. The device comprised of three principle components: the lithium niobate-based SAW device, the nanopatterned polymeric layer with an array of 500 nm cavities, and the microchannel in which bead solutions were introduced and removed. During operation of this acoustofluidic device, millions of beads were simultaneously directed and held in single-particle traps. In doing so, we overcome the hitherto inseparable coupling between the applied acoustic wavelength and the length scale of the resulting force gradients. Microfluidic channels are used to contain a solution of submicron particles on top of a patterned nanocavity array, below which is a traveling SAW device. After applying a moving SAW, the nanocavity deformation is induced by the oscillatory displacement of the underlying SAW device, which couples with the surrounding fluid to generate a time-averaged pressure field that guides the suspended particles to a pressure minimum by the acoustic radiation force, as shown by Figure 2.3. Traveling SAWs produce nonzero, time-averaged

pressure fields which can direct particles in the direction of wave propagation or toward local minima of a near field interference pattern. Here, however, the oscillating nanocavities give rise to local minima in the time-averaged pressure field within each nanocavity, to which suspended particles are directed by an acoustic radiation force. Using SAW wavelengths between 20 and 80 µm to generate nanoscale acoustic gradients in the vicinity of a single nanocavity, 300 nm diameter particles were successfully trapped within a 500 nm diameter cavity by applying a traveling SAW.

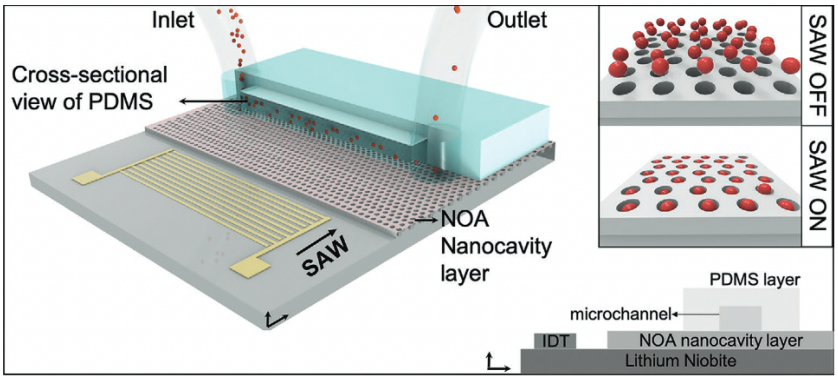


Figure 2.3: Structure of the SAW/nanocavity layer device. With the SAW device turned on, beads are trapped by the cavities. When SAW device is turned off, the beads are released from the cavities.

## 2.3 Comparison between two method of manipulating beads

In the Equation 2.2, v is sound velocity in lithium niobate that equals 3995 m/s [12] and $\lambda$ is SAW wavelength that equals pitch of IDTs. According to Equation 2.2, it is easy to calculate the resonance frequency of the device in order to manipulate objects in micron scales with standing surface acoustic wave. Table 2.1 shows the frequencies been calculated to manipulate different size of objects. The first four columns show the different size of objects to be manipulated by standing wave. The last column shows that 300 nm objects to be manipulated by 200 MHz traveling wave coupled with cavities. In the case of manipulating with frequency of several GHz, it is a challenge to fabricate surface acoustic wave devices as it requires very fine precision fabrication. However, the application of surface acoustic waves coupled to nano-structures can reduce the need for high desired frequencies to manipulate sub-micron objects.

$$f = v/\lambda \tag{2.2}$$

| | Standing wave | | | | Traveling wave/nano-structure |
|---|---|---|---|---|---|
| Size | 10nm | 100nm | $1\mu m$ | $10\mu m$ | 300 nm |
| Freq | 400 GHz | 40 GHz | 4 GHz | 400 MHz | 200 MHz |

Table 2.1: First four columns are different size of objects manipulated by standing wave. The last column shows the required frequency for traveling wave coupled with nano-structure to manipulate 300 nm objects.

## 2.4 Research question and Objectives

In this project we hypothesize that multiplexing can be achieved by acoustically controlling the on-chip position of microbeads on nanopore chips. Each bead in turn positions the tethered biomolecule right above the nanopore sensing region. This active delivery has the advantage that it firstly provides a speed control mechanism, since the motion of the biomolecule in the nanopore can be controlled by the positioning of the bead compared to free diffusion. Secondly, it can offer multiplexing capabilities if the many beads can be accurately and simultaneously be localized above the nanopore sensors.

In this project we will therefore address the following research question: **Can nanoscale acoustic force gradients manipulate submicron-beads in-plane on a nanopore sequencing device?**

We will take a multi-step approach to test the feasibility of this acoustic localization mechanism and have organized the project to attain three main objectives.

**Objective 1. Fabricate an array of cavities on piezoelectric lithium niobate substrates**

This includes designing and generating micron-sized cavities and characterizing their geometry and topography (i.e. symmetry, surface roughness etc). As mentioned early, microcavity layer can bring operating frequency down to few hundred MHz. A proper microcavity layer model demonstrated by running in COMSOl is necessary. Meanwhile, microcavity layer need to be strictly fabricated by following the COMSOL model. These parameters during fabrication process need to be repeatedly verified.

**Objective 2. Characterization of SAW devices with a cavity layer**

In this part the aim is to test the performance of LN-based SAW devices with and without cavities by carrying out scattering (S) parameter measurements. It is crucial to have SAW device with the desired resonance frequency to enable parallel particle manipulation. As mentioned earlier, scattering parameter provide information on SAW device performance. Specifically, the S11 and S21 parameters represent the reflection and transmission of the acoustic wave in a two port device. In this case, a vector network analyser (VNA) is widely used to measure the S parameters. Important parameters that need to be optimized for this device are the cavity array geometry (diameter, depth and pitch) relative to the acoustic

wavelength. To guide the design of the devices, we will perform COMSOL simulations. These simulations will be used to predict the frequency response of the SAW device and the acoustic pressure fields produced in the presence of the cavity array and the results will be compared with result from VNA measuremenrs to evaluate the accuracy of the model.

**Objective 3. Demonstrate acoustic trapping microbeads by fluorescence imaging during SAW actuation**

Once the device is fabricated with the optimized cavity array design (objectives 1 and 2) we will investigate the actuation of microbeads in solution in the device. In practice, this means observing whether the microbeads are acoustically trapped on the surface of the chip and specifically one bead per cavity. If the device operates as required, the microbeads should produce a pattern which can easily be visualized using fluorescence microscopy during SAW actuation. We will check if this process is reversible and over how many cycles. To determine the trapping efficiency, we will count the ratio of trapped beads for different acoustic wavelengths. Previous work indicated that the relation between the acoustic wavelength and the cavity array geometry is key to produce high trapping efficiencies, as this directly impacts the generated acoustic pressure fields.

# 3 Methods

This chapter explains the techniques, materials and instruments used to achieve the fabrication, measurement and characterization of device. First, the whole device and trapping experiment can be considered as three major components according to their function: 1. The NOA (Norland Optical Adhesive) layer cavity array 2. The SAW device and 3. The fluorescence imaging system to visualize bead behaviour during actuation.

## 3.1 Atomic force microscopy (AFM)

Atomic force microscopy is a high resolution type of scanning force microscopy techniques, which has the microfabricated cantilever with fine tip attached to its free end. Through scanning the surface with the sharp tip, the sample topography can be reconstructed.[13]

In a measurement, the scanning mode of the tip can determine the accuracy of the results. However, different modes are selected to scan different types of surface. For contact mode, tip directly contact the surface during the scanning. The distance between tip and surface is adjusted by the electric feedback loop, which has elastic repulsion force as input.[15] Since the tip directly contacts the sample, it can cause the damage on the surface of sample. When using non-contacts mode tip to scan the surface, cantilever is vibrating at its resonance frequency. By changing the amplitude and phase of the vibration, it is possible to keep the constant of distance between tip and sample. Meanwhile, the non-contact mode tip does not make any damage on the sample surface. In this case, scanning with the contact mode tip has much higher resolution than it scanning with non-contact mode tip. Hence, the tapping mode was designed to neutralize the characterization of contact mode and non-contacts mode. Therefore, scanning with tapping mode is able to achieve higher resolution than non-contact mode and less damage than contact mode.

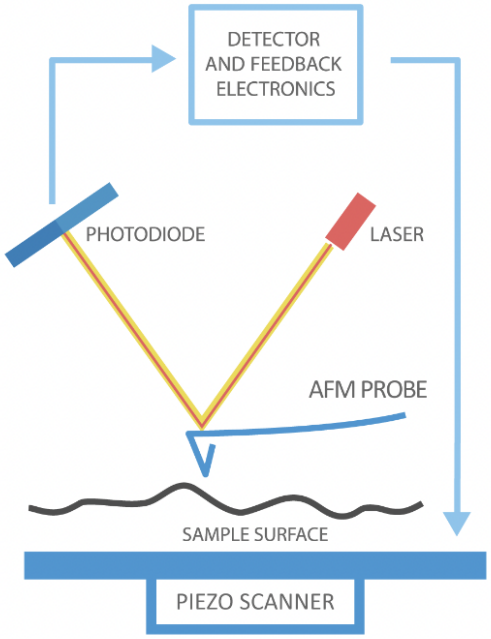


Figure 3.1: Atomic force microscopy schematic. The laser is reflected off the end of cantilever and detected by photo detector.[14]

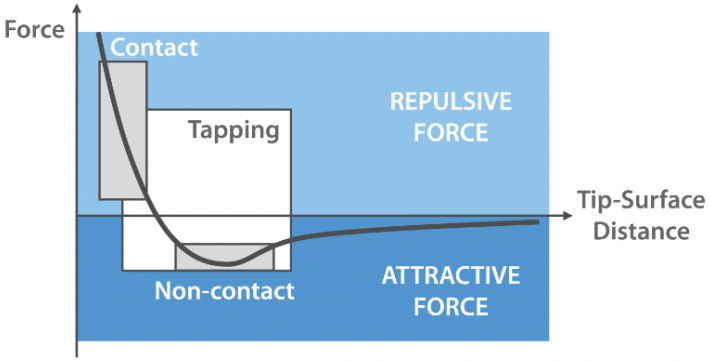


Figure 3.2: Operation regions for Contact, Tapping and Non-Contact Mode[14]

## 3.2 Producing a NOA layer with embedded nanocavity array

This section aims to develop a method to produce NOA polymer layers with uniform thickness in which an array of cavities with reproducible dimensions can be generated. In the

experiment, NOA81 is used as the material of polymer layer. It is a liquid adhesive that cures in seconds to a tough, hard polymer when exposed to ultraviolet light. We will determine the thickness of the layer, as well as the depth, shape and pitch of the cavity array.

Since the beads used for the fluorescence imaging experiment are 1.5 $\mu m$ in diameter, the thickness of the NOA layer cannot be less than 2 $\mu m$. As the surface acoustic wave will be traveling along the top surface of substrate, and its power dramatically decreases in the bulk direction, it is better to have cavities' bottom close to top surface of substrate.

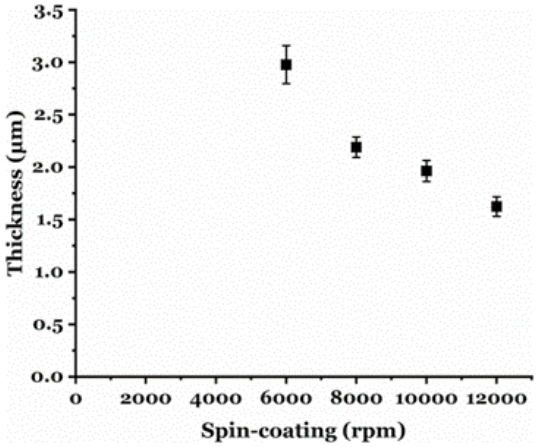


Figure 3.3: Relationship between thickness of NOA81 film and spin speed.[16]

Figure 3.3 gives an approximate relationship between thickness and spin speed which is used as reference for further experiments. We aimed to achieve 2 $\mu m$ thick NOA film so that bottoms of cavities are not too far from the substrate. Hence, the range of spin speed that has been selected is between 7000 to 8000 rpm. The procedures of NOA film deposition and thickness measurement were as follow. First, spin coat a NOA film onto the substrate with 7000 to 8000 rpm for spin speed. Then, expose the substrate to a UV light source for 1 minute to cure the film. Finally, make a cut through the NOA film with a sharp scalpel and use AFM or white light interference to scan the profile of the surface. To analyze the results, compare the measured data with the data from line graph and confirm the fact that 7000 to 8000 rpm for spin speed can produce the NOA film with 2 $\mu m$ in thickness. However, if experiment results do not act like the line graph, the target speed could be found through multiple experiments.

## 3.3 Cavity Array fabrication

There are two methods to generate cavity arrays in the deposited NOA layer: namely femtosecond laser cutting and two photon polymerization. These are a subtractive and additive technique respectively.

### 3.3.1 Cavity arrays made by femetosecond laser cutting

Using a combination of a high numerical aperture objective, a short wavelength light source (e.g. ultra violet) and a femtosecond laser pulse duration, sharp and well-defined microstructures of a few micrometers can be produced by laser manufacturing. [17]

In the laser cutting system, many parameters directly determine the dimension of the cavities.

- First of all, in order to create features in the NOA layer, we need to make a design that is compatible with the laser cutting system. The drawings for cavities are circles with pre-defined diameters and pitch.
- Determine the values of speed and jump speed. The speed of the laser movement determined time has been used for cutting each feature. Furthermore, the jump speed determines the time that is used to move the laser spot from one feature to another. If it is too small then it will cause drag marks.
- Additionally, there are two crucial parameters affecting dimension of cavities which are laser power and repetition.
- At last, focus on the top surface and laser cut it.

The optimization of the cavity structures will be shown in chapter 4.2.1.

### 3.3.2 Cavity arrays made by two photon polymerization

Two-photon polymerization is a type of additive manufacturing technique that can print nanostructures by polymerizing photoresponsive material. It enables very high spatial resolution, with features smaller than Abbe's diffraction limit being produced due to non-linear light-induced effects in the photoresponsive material.[18; 19; 20] Figure 3.4 shows the two types of configuration of the objective and the substrate. The left configuration is better suited for thinner substrates, while the right figure is employed for thicker substrate. The change in configuration depends on the thickness due to the maximum working distance of

the objective of 360 $\mu$m. Hence, for substrates thicker than this limit, the photoresponsive material must be placed underneath the substrate as shown in Figure 3.4(b).

For the two-photon lithography approach we will perform the following tasks:

- Design a model (Figure 3.5) in Solidworks and convert it into code that can be run by the machine.
- Prepare samples. We clean the substrate with IPA and place the substrate on a sample holder. Following that, place a droplet of resin on the substrate.
- Place the sample holder such that the droplet faces downwards and contacts the objective lens.
- After the features are printed, submerge in the developer PGMEA for 25 min to remove the unpolymerized regions. Then put the sample in IPA for 5 min so that residual PGMEA can is removed. Finally, dry the sample with an air gun, and the chip is ready to be used.

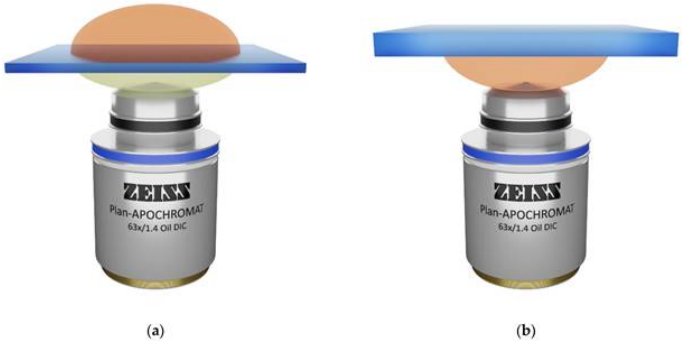


Figure 3.4: Schematic of the two types of arrangements for 2PP printing. **a)** The printing region is above the thinner substrate. **b)** The printing region is below the thicker substrate.

## 3.4 SAW device characterization

S-parameters are important to characterize and assess the performance of a SAW device. Among other things, they enable the extraction of the resonance frequency of the device during operation.

For a simple two port system such as the one shown in Figure 3.6 a), S-parameter generally can be described as [21]. S11 is the input reflection coefficient; S12 is the reverse transmission coefficient; S21 is the forward transmission coefficient; S22 is the output reflection coefficient. These S parameters can be measured using a vector network analyzer and during this project a nanoVNA was used (Figure 3.6 b)). Measured $S_{21}$ and $S_{11}$ data are stored as an s2p file,

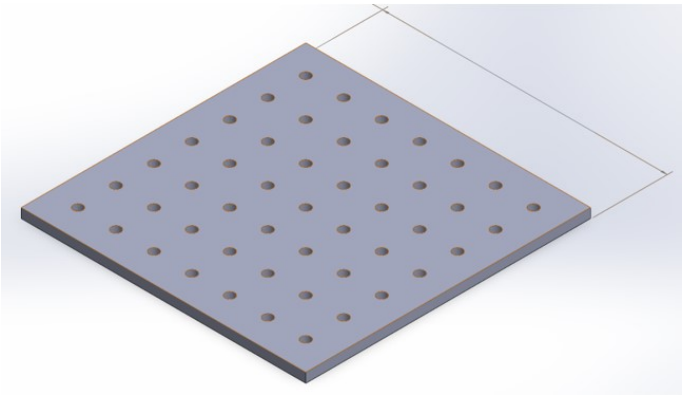

Figure 3.5: Two photon polymerization printing model with cavities of 2 $\mu m$ width and 1.5 $\mu m$ depth.

and further analysed using a Matlab script. An approximate value for resonance frequency can be estimated from the Equation 2.2.

Once the expected value is extracted, a measurement is performed in the frequency range which includes the resonance frequency.

$$\begin{bmatrix} b_1 \\ b_2 \end{bmatrix} = \begin{bmatrix} S_{11} & S_{12} \\ S_{21} & S_{22} \end{bmatrix} \begin{bmatrix} a_1 \\ a_2 \end{bmatrix} \tag{3.1}$$

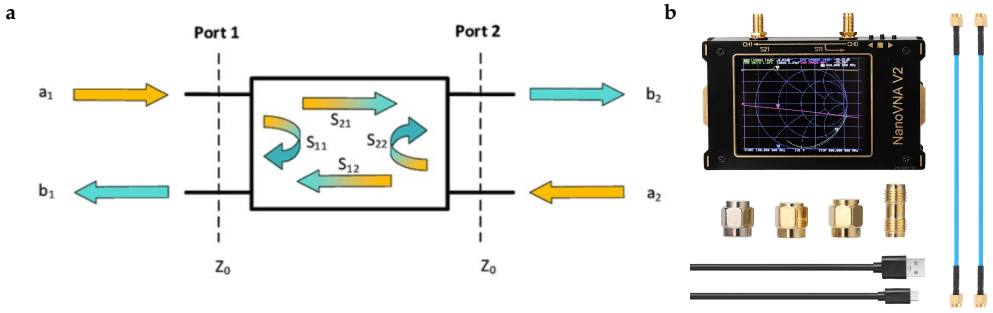


Figure 3.6: (a) Two port network where a1 a2 are incident waves, b1 b2 are reflected wave.[22] (b) NanoVNA for measuring S parameter.

## 3.5 Fluorescence imaging

Fluorescence imaging is a versatile and non-invasive way to visualize the live motion of micron scale objects in space and time. It relies on the use of stains and dyes that are

attached to the objects of interest (usually via chemical bonding) and are excited by specific wavelengths. They then re-emit light at a longer wavelength which can be detected by eye or by a camera.[23] It is a big advantage to visualize nano scale bio-molecules which are smaller than visible light wavelength. The emitted light wavelength is typically in 300 - 800 nm. In this project we use an inverted epifluorescennce microscope as shown in Figure 3.7 a) to monitor the response of fluorescent microbeads during actuation. There are two wavelength filters available in this microscope: 470 nm and 525 nm. We note that for accurate monitoring of the bead position and motion, we have to ensure that the components of the SAW device and flow cell do no auto-fluoresce in the same wavelength as the beads as this will render the beads indistiguishable from the surroundings. As Figure 3.7 b), when fluorescence dyes absorb lights, the energy of molecule is raised up to a higher excited state. The wavelength of re-emit light was determined by types of dyes being used.

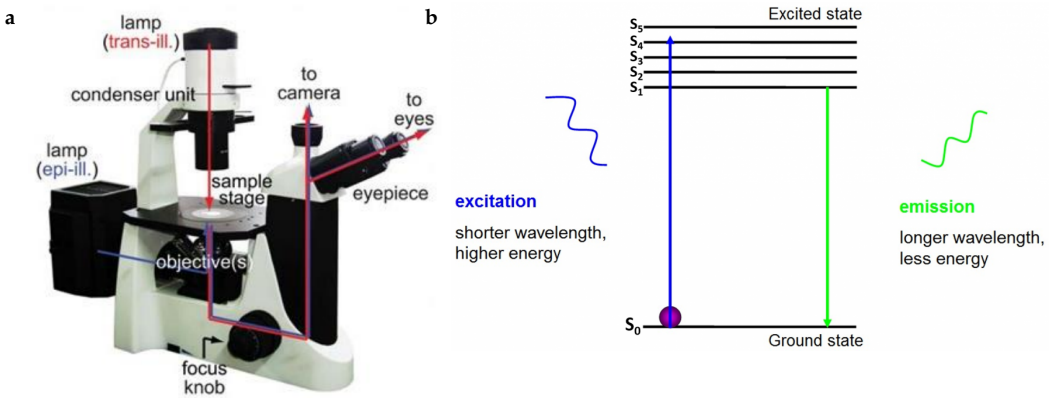


Figure 3.7: **a)** Inverted microscope with both bright-field and fluorescence microscopy modes. The blue lines represent the optical path for trans- illumination microscopy and the red lines is epi-illumination microscopy. **b)** Schematic of the fluorescence process: fluorescent materials absorb excitation light to excited electronic states and then re-emitting fluorescence light.[24]

# 4 Results

In this chapter, we first discuss the NOA layer thickness and cavity profile fabricated with two different approaches, laser milling and two photon polymerization. Then, we set up, generate and interpret acoustic pressure distribution from the COMSOL simulations and compare measured and simulated results for S-parameter characterization. Finally, we present microbeads trapping with and without acoustic actuation.

## 4.1 NOA layer profile

In order to measure the thickness of the NOA film after deposition, spin coating and UV baking, we made a cut in the film with a scalpel. By using the white light interferometry and focusing on the edge of cut film, the profile of the NOA layer can be easily scanned. We tested spin speed in the range of 7000 rpm to 9000 rpm. All the experiments for thickness testing were done on clean lithium niobate substrates. Figure 4.1 shows the interferometry image where the orange region on the left is the NOA layer and the blue region on the right is the bare LN substrate.

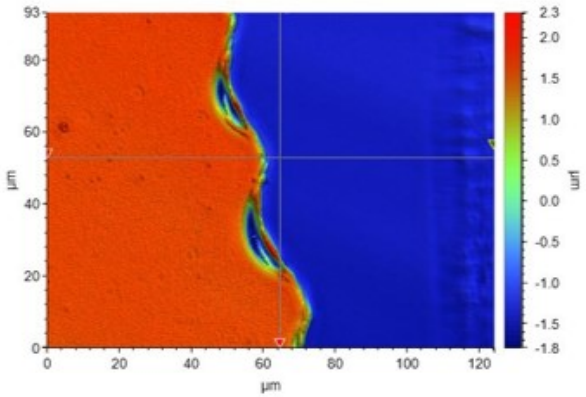


Figure 4.1: Optical interferometry image of the coated LN substrate, where the orange region is the NOA layer and the blue region is LN substrate.

Figure 4.2 shows the height profile at the edge of the NOA film measured with a profilometer, from which we extract a height of 2.72 $\mu m$ with 7000 rpm for spin speed. Additionally, over a region of 60 $\mu m$ the film has relatively uniform height, as shown by the consistent shading over the area.

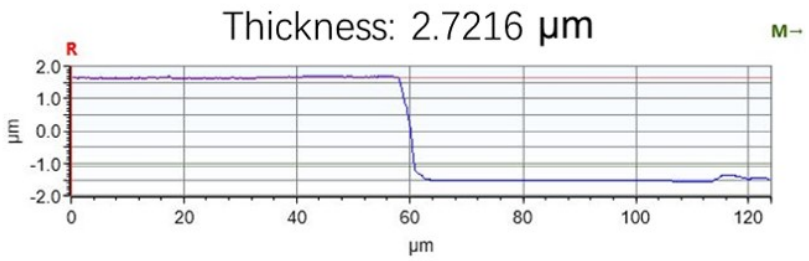


Figure 4.2: Profile of layer thickness is shown in the picture, and was scanned from left to right. The thickness of NOA layer is around 2.72 $\mu m$.

## 4.2 Cavity array fabrication

### 4.2.1 Cavities made by femtosecond laser cutting

The procedure developed for laser cutting cavities can be described as follows:

1. Import the drawing of features or directly make the drawing in the femtosecond laser system.

2. Define the size of the feature by its length, width.

3. Two more essential parameters must be defined: power and repetition. The power determines the proportion of the total laser being excited, and repetition means how many times the features are cut. These two parameters also indirectly affect the dimension of cavities (i.e. Higher power laser usually burns more materials). Hence, the combination of different scales for these two parameters must be demonstrated. Finally, the recipe of different parameters is demonstrated by the experiment and applied in real device fabrication.

The first cavity characterization experiment is meant to find the combination of power and repetition that can enable manufacturing of the target dimension of the cavities (i.e. 2 $\mu m$ in depth and width.). Hence, we perform a dose test and adjust the parameters in an array changing one parameters along the rows and another parameter along the columns. (Figure 4.3) shows a 10 x 10 matrix with power of the laser increasing in the positive y direction and repetition increasing in the positive x direction. Both power and repetition

increased from 1 to 19 with the step size of 2. Once cavities are selected from the matrix for post-fabrication characterization, power and repetition parameters are known from their row and column numbers.

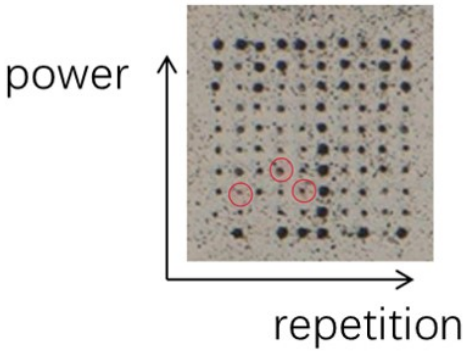


Figure 4.3: Power of laser increasing in positive y direction and repetition increasing in positive x direction. Both power and repetition are in range of 1 to 19 with an increment of two per step. Three cavities are selected for subsequent characterization as indicated by red circles.

AFM is a powerful tool used here to map the profile of cavities. By analyzing the profiles, we can select cavities that most have the desired dimensions and use the same parameters to produce uniform arrays of cavities with the same properties. Four cavities were selected from the cavity matrix in Figure 4.3 for further characterization. Cavity d), e) and f) were located close to the origin, cavity in Figure 4.5 was located much further away. Considering the size of the fluorescent beads, cavities e) and f) are better suited to the actuation experiments. The dimensions of both e) and (f) fit one bead per cavity. However, cavity d) is too small to fit a bead. Cavities located at the right corner of the cavity matrix are bigger than cavities in Figure 4.4. By looking at the AFM topography Figure 4.5 b), the bottom of the cavity is too flat, and there is no noise which means the tip is scanning the air rather than the cavity floor. Hence, this cavity is too deep to be measured with AFM. Another feature of cavities made by femtosecond laser cutting is their characteristic v-shape. This feature can be well explained by considering Gaussian laser beam profile.

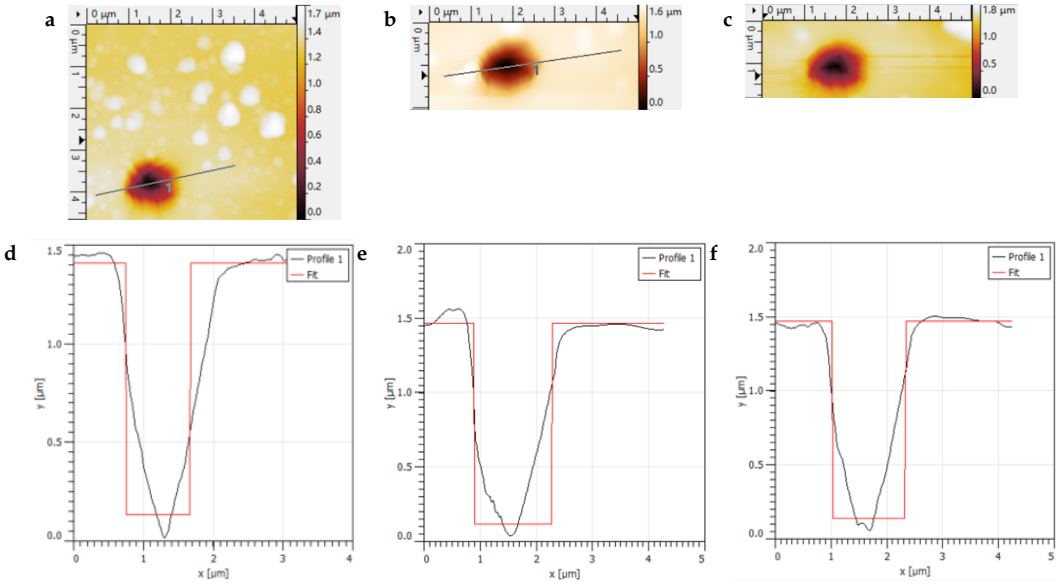


Figure 4.4: a), b), c) are AFM topography images of the cavities in row 3 column 2; row 3 column 5; row 4 column 4, respectively. d), e), f) are the corresponding profiles taken at the position of the solid lines in the AFM images. The widths and depths of the cavities are: 1.578 $\mu m$ and 1.373 $\mu m$ for cavity A, in width and in depth, e) is 1.762 $\mu m$ in width and 1.433 $\mu m$ in depth, f) is 1.854 $\mu m$ in width and 1.388 $\mu m$ in depth.

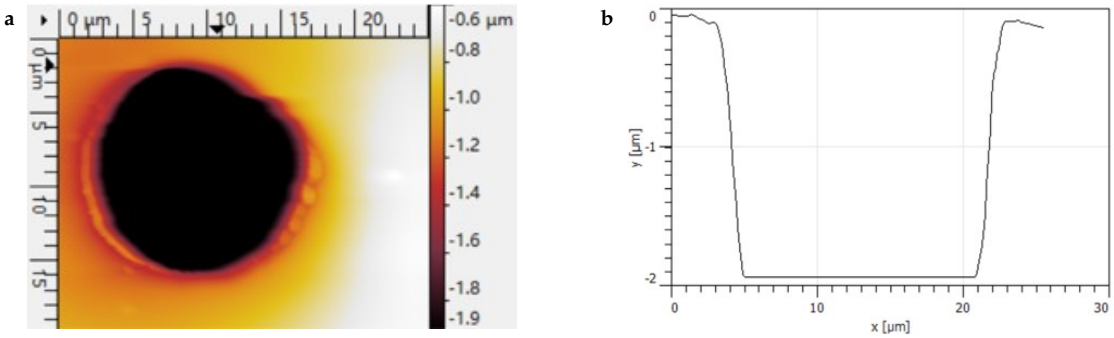


Figure 4.5: a) AFM image of the large cavity located at right top corner of the cavity matrix. b) Profile of the cavity across its diameter.

### 4.2.2 Cavities made by two photon polymerization

Since two-photon polymerization is an additive manufacturing method, it has the advantage that printed features are more precise than laser-cut features. Figure 4.6 show the AFM topography image and profile of a two-photon polymerization printed cavity layer. The cav-

ities' side view shape is closer to rectangular with straighter walls than in the femtosecond laser cutting case. The dimension of all cavities are uniform. However, the depths of cavities are 1.157 $\mu m$, even though they were designed with 1.5 $\mu m$ in depth. By further understanding the principle of printing features with two-photon polymerization, it is easy to find that some printing material loss can enhance the adhesion between printed feature and substrate. This error can be easily avoided by taking it into consideration while designing the model.

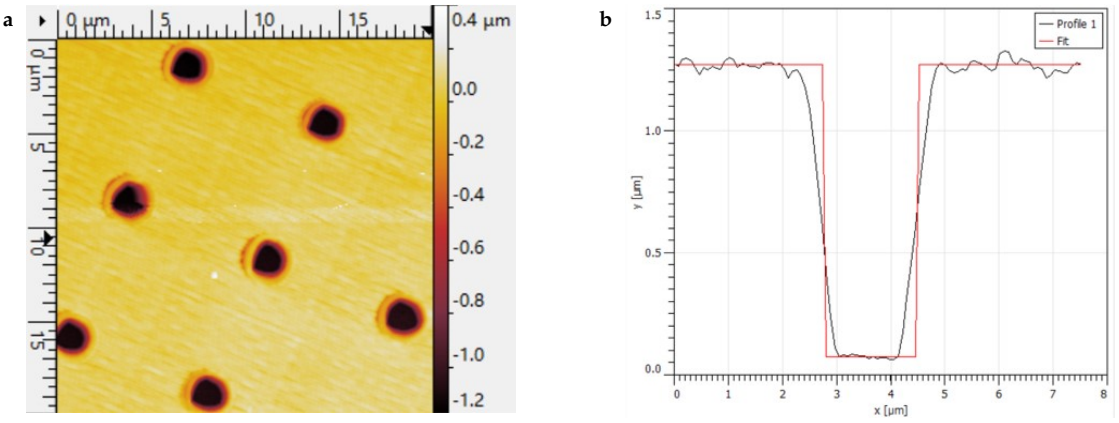


Figure 4.6: a) AFM image of the two photon polymerization printed cavity. b) Profile of the cavity. Depth:1.157 $\mu m$ and designed depth: 1.5 $\mu m$

Figure 4.7 a) shows the fluorescence image of cavity layer imaged in the inverted microscope with the 470 nm filter. The arrays (bright green squares) appear very bright against the background. This is the case for all features produced with the 2PP technique and can be traced back to 1997.[25] In general, the materials used in two photon polymerization consist of a mixture of monomers and oligomers. These materials are cross-linked throughout the radical photopolymerization provided by photoinitiator.[25] However, mostly common used photoinitiator are exhibiting autofluorescence, which also hinders the application of the technology in many researches that use fluorescence microscope.

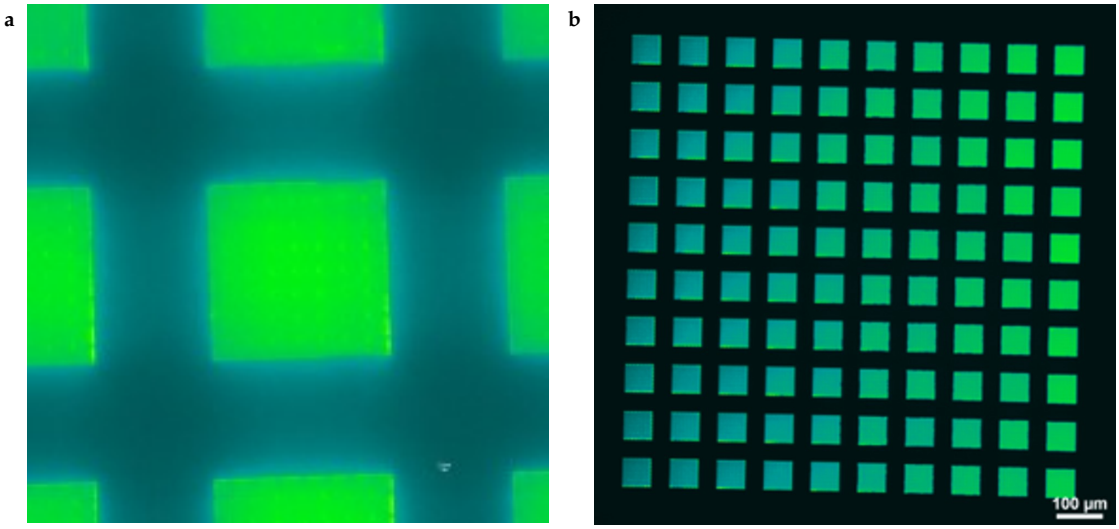


Figure 4.7: a) Image of the cavity array taken in the inverted fluorescence microscope with 470 nm wavelength filter. The resin as printing material was self-fluorescent in the same wavelegth as the beads. b) Zoomed out view of cavity. array

## 4.3 COMSOL multi-physics

Before discussing the SAW device characterization and actuation, some simulations were done in COMSOL. This section will treat two aspects: 1. S-parameter simulations, which can provide a reference for the subsequent electrical characterization, and 2. the acoustic pressure distribution generated by the presence of the cavities, which helps optimize the design and experimental parameters for optimal trapping capabilities.

### 4.3.1 S-parameter simulation

We execute a frequency domain study in two dimensions using the Solid Mechanics, Electrostatics, and Multiphysics Piezoelectric Effect physics interfaces. The simulated geometry consists of Au IDT domains and LN domains. In Solid Mechanics Physics, the Au and LN domains are assigned to the Linear Elastic Materials and Piezoelectric Materials nodes, respectively. The fingers of IDTs are alternately connected to the ground or the RF source. In the simulation, gold domains are assigned to a terminated terminal and a zero-voltage terminal node. The terminated terminal type allows for a calculation of the S-parameters in the frequency domain study. In our model, there are three Terminals where two of them are for the generation and reception of surface acoustic wave, and the rest is connected to

ground. The reference impedance Zref is set to 50 Ω. Lastly, the LN domain is assigned to the Piezoelectric node. The results that came out of the study are the displacement field, electric field, and terminal voltages. In chapter 4.4, the S parameter results will be discussed, and $S_{21}$ plot will be shown.

### 4.3.2 Acoustic pressure distribution

Next, we execute a Frequency Domain study in two dimensions model with only the substrate, cavity layer, and water field. With a combination of two types of physics, solid mechanics and thermoviscous acoustic, the acoustic pressure distribution can be simulated.

A first simple model has been designed with two cavities only. It is possible to calculate the differences between pressure inside and outside the cavities by analyzing the map of acoustic pressure distribution. The model consists of two cavities that have 2 $\mu m$ for both width and depth. The interval between two cavities is 10 $\mu m$. Except for the number of cavities, all parameters in this simulation are the same as in the real device. We performed the simulation in the frequency range from 300 to 400 MHz in steps of 10 MHz. This step is carried out to compare the results obtained at different operational frequencies. Figure 4.9a shows the acoustic pressure distribution at 340 MHz.

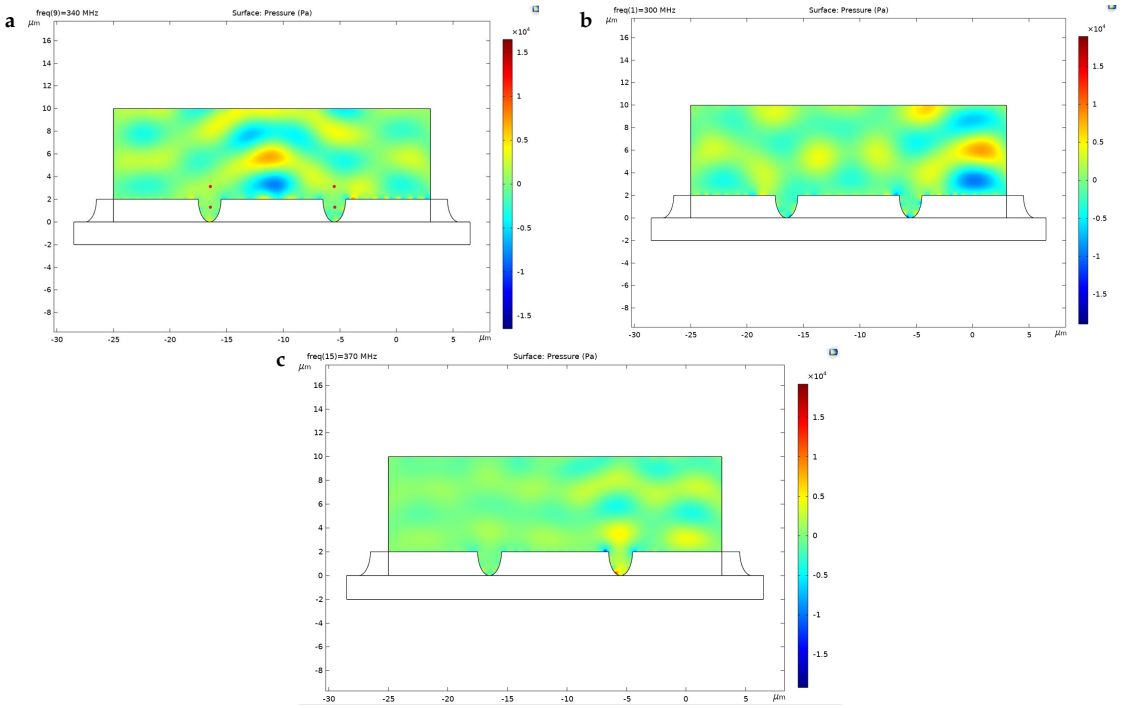


Figure 4.8: a)Pressure of four positions has been measured from the acoustic pressure map; 340 MHz b) 300 MHz c) 370 MHz

Based on the results, we intend to evaluate the ability to trap beads under different frequencies. In doing so, we selected two points at the position of each cavity and exported acoustic pressure data, respectively. Hence, there are four points that have been selected for each frequency. Since we only manipulate beads in the plane, we picked the position of one of the points (label it as the second point) at 1 $\mu m$ above the cavity, which is 3 $\mu m$ for its y value. The position for the other point (label it as the first point) is sitting in the middle of the cavity. Both points are illustrated as red point. In the pressure data sheet, we extracted the pressure difference for each cavity by subtracting the pressure at the second point from the first point. This value needs to be negative in order to get beads trapped. A bar chart (Figure 4.9) was made to display the pressure differences for each frequency. All the positive y values mean that pressure in the cavity is greater than the outside. Conversely, a negative value means that pressure outside the cavity is greater than the inside. Based on Figure 4.9, the device showed better beads capture performance when driving at 300, 340, and 370 MHz. Figure 4.10 shows the acoustic pressure distribution but with rectangular shape cavities. These results in a big change compared to v-shape cavities pressure maps. However, through measurements, the pressure difference is still negative which means beads should be trapped.

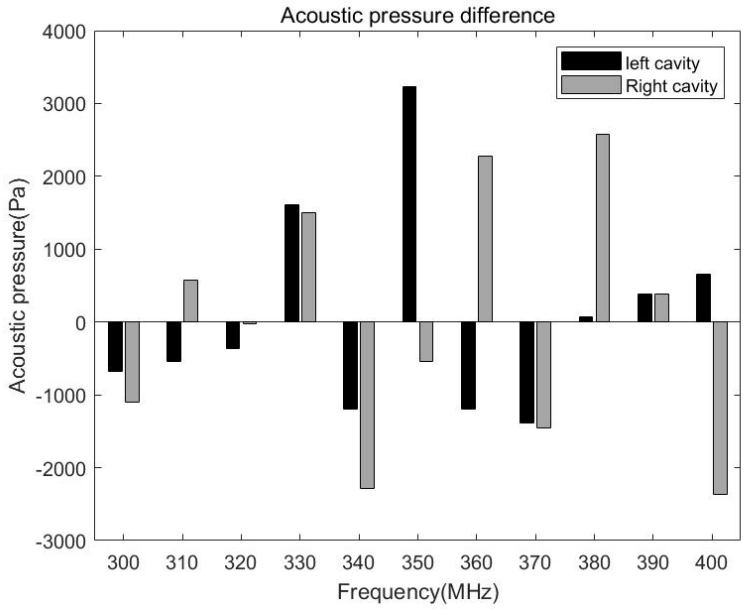


Figure 4.9: Bar chart of the pressure difference betwene the outside and inside of the cavities. Black and grey represent left and right cavity respectively. Negative values mean that the pressure in the cavity is smaller.

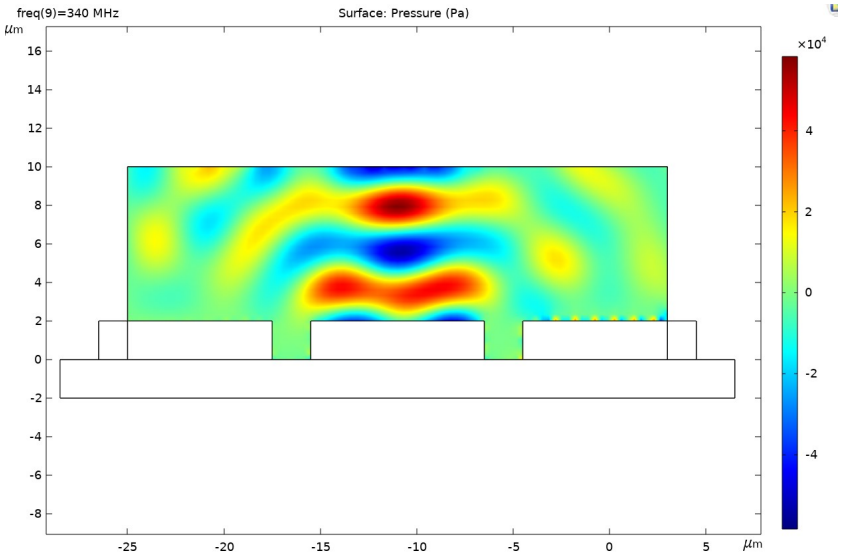


Figure 4.10: Acoustic pressure map with rectangular shape cavities

## 4.4 Surface acoustic wave devices characterization

To measure the S parameters, the SAW device needs to be connected to nanoVNA as seen in Figure 3.6(b). Therefore, A printed circuit board (PCB) was used to connect the nanoVNA and SAW device. On a LN chip, we patterned 2 sets of IDTs and 2 individual IDTs. At least one set of IDTs is necessary to measure the S parameters. Any individual IDTs can be used to actuate objects. One set of the IDTs is wire bonded to the PCB in order to measure the S parameters.

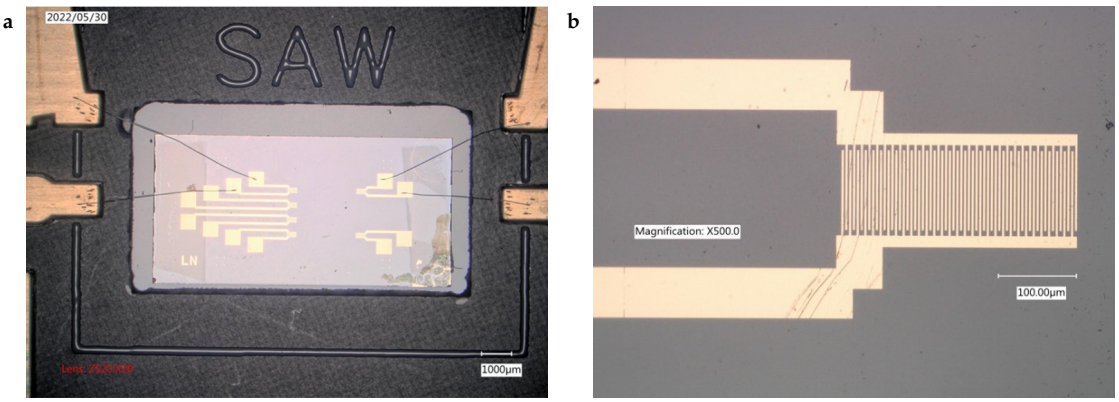


Figure 4.11: a) One set of IDTs was wire bonded to the PCB in order to measure the S-parameter. b) Zoomed in view of one IDTs.

For each IDTs, there are two terminals, and both terminals constitute one port. Usually, port 1 is considered as input port, and port 2 is considered as output port. To test whether the device is functional we measured the S21 of the device, which can directly tell us the resonance frequency and how much energy is transferred. The measurements are then compared with the simulated S parameters. Simulations were run from 300 MHz to 450 MHz with a frequency step of 100 kHz. We find a good agreement between simulation and experiments both in terms of magnitude and shape of the electrical response of the device, as shown in Figure 4.13a. Both measurement and simulation results reached the same amount of peak power ratio at the same resonance frequency, validating both our model and the fabrication procedure.

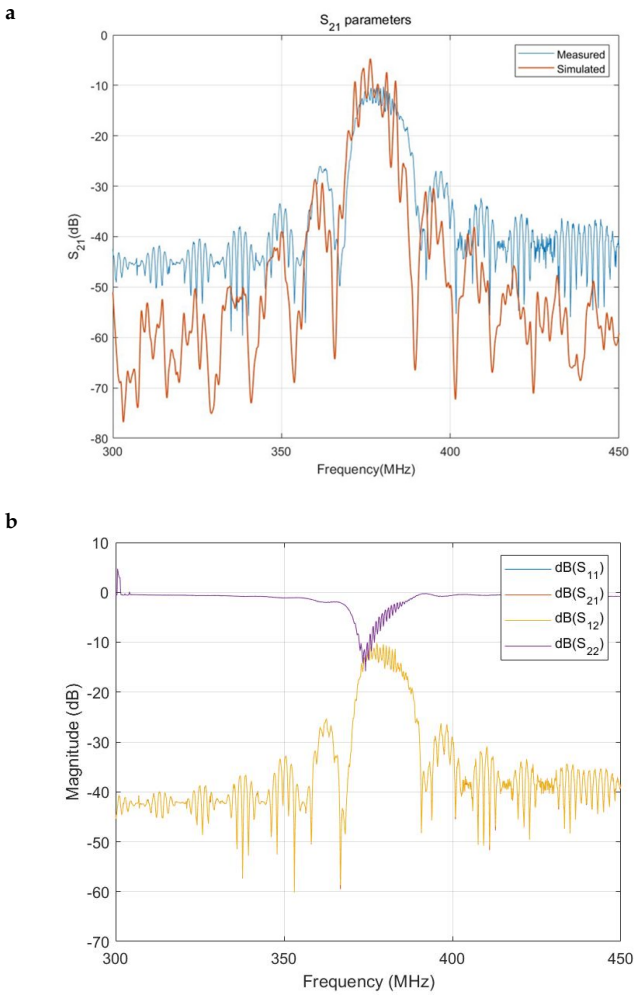


Figure 4.12: a) Comparison between simulated (red) and measured (blue) magnitude frequency response ($S_{21}$) for the device from 300 MHz to 450 MHz. b) S parameter plot of the device with a NOA nanocavity layer.

## 4.5 Microbeads motion without actuation

This section reports the motion of fluorescence beads on the cavity layer. Instead of connecting the SAW device to the signal generator, we put a droplet of fluorescence beads solution diluted 100 times with Milli-Q water and let it settle for around 15 minutes. Then observe it under the fluorescence microscope.

During this period there were not many fluorescence beads trapped in cavities. Tiny beads in a stationary droplet do not behave like they do in a flowing liquid, which can be explained by Brownian motion. As famously explained by Albert Einstein in 1905, it is a process during which tiny beads move randomly in a homogeneous isotropic fluid as they experience independent molecular collisions from the thermally excited fluid molecules.[26] In the absence of any actuation, there is no effect of cavities on the particles. However, after the droplet dried, some fluorescence beads were found filling a cavity.

Figure 4.13 shows the location of the cavity matrix, and some of the beads on the surface are also visible. By closely looking at the first left column, we can notice that cavities are slightly greater than the rest due to the misfocused laser.

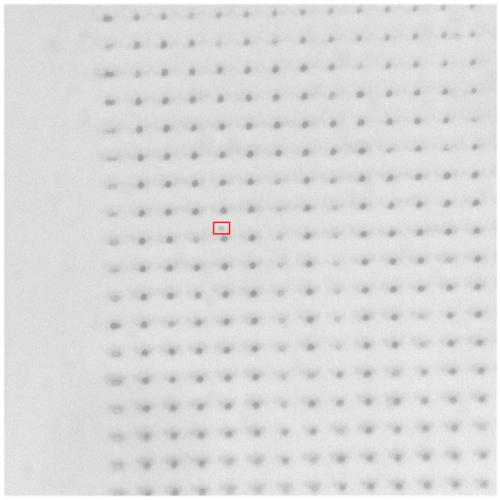

Figure 4.13: Observing the fluorescence beads on cavity layer under the white light field.

Figure 4.14 is a fluorescence image taken with the 470 nm filter, illustrating that there is a line of brighter spots in the first, left-most column because more than one fluorescence bead is trapped in most cavities of the first column. There are fewer bright spots at the top part of the matrix for the normal size of cavities.

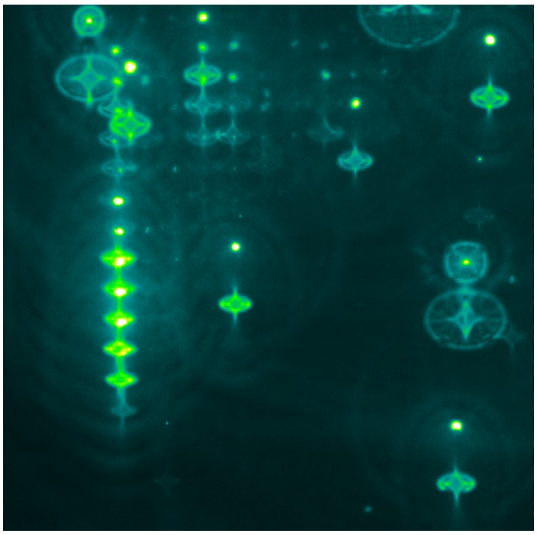

Figure 4.14: Observing the fluorescence beads on cavity layer with 470 nm wavelength fluorescence light.

## 4.6 Microbeads trapping with actuation

All the previous experiments were done with dummy lithium niobate chip containing cavities. In this section, we will discuss the results collected from the device and observe the microbeads reaction during acoustic actuation. To fabricate device with NOA layer and get it ready for laser cutting, it is slightly different from spin coating a layer on top of the dummy chip. Following the steps shown in Figure 4.15, and to avoid the NOA material cover the IDTs, we used gel material to cover the IDTs first. Then, put a droplet of NOA material covering the device and spin coat. After curing it by exposing the entire device under the UV light for 2 mins, we could eventually get a NOA layer in between opposing IDTs.

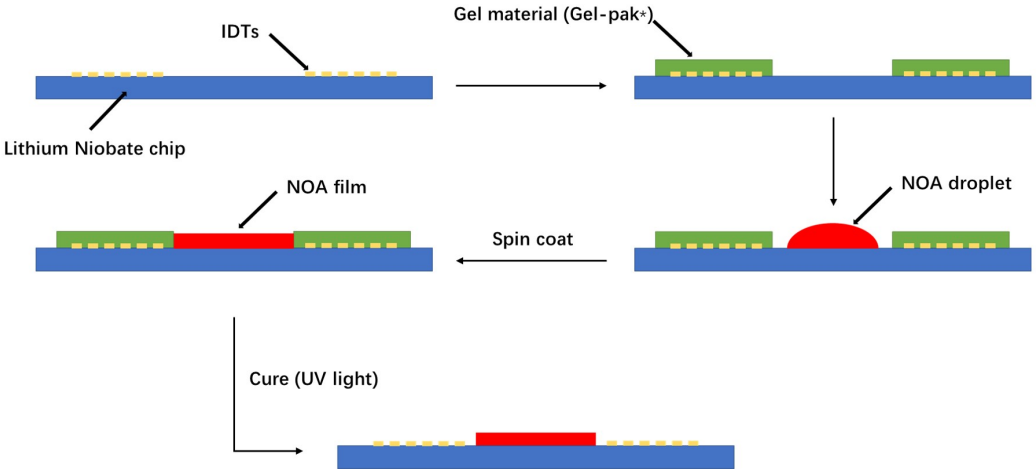


Figure 4.15: The procedure of spin coating a NOA layer in between two conflict IDTs.

Three devices were made in total for testing microbeads trapping. They are named as device 1, 2 and 3. During the first actuation experiment, device 1 was driven under 360 MHz to 390 MHz for frequency and 0 to 10 dBm for power. As shown in the Figure 4.16 a, 1 mm wide NOA film was spin-coated onto the SAW device and in between each set of IDTs. After that, four matrices of cavities were cut on the film by femtosecond laser. However, there are imperfections in the zoomed in view Figure 4.16 b of cavity matrix. Since the whole NOA surface is not in focus during laser cutting, the array was not properly milled and did not appear on the surface. An additional reason why imperfections are generated will be discussed in chapter 5. Then a solution of 1.5 $\mu m$ fluorescence beads was prepared. we extract 4 $\mu L$ liquid and drop it on top of cavities. There is only one IDTs in connection with function generator which can produce traveling surface acoustic wave while actuating the device.

In the first actuation experiment, it was found that no patterning of fluorescence beads was observed. Figure 4.17 shows the captured fluorescence image of microbeads located on the surface during actuation. By adjusting the knob of microscope, we explored more of beads are flowing in the bulk. Meanwhile, it was easy to notice that they were moving faster than those located on the surface during the actuation. The streaming beads tend to move away from the IDTs and go a round trip back to the original position. The velocities for both beads on the surface and in bulk linearly depend on RF power. High velocities were observed for higher power.

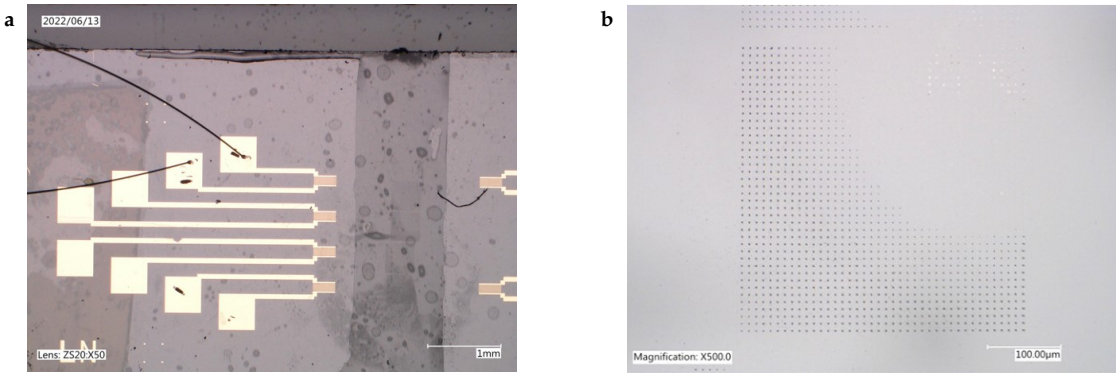


Figure 4.16: a) Top view of the real device. There are 4 IDTs on the left side and two IDTs on the right side. Every two opposing IDTs become a set of IDTs which was used during measuring the S parameter. The cavities layer is in between the SAW device in darker grey. b) Since the thickness of the layer was non-uniform, part of the cavities array was missed.

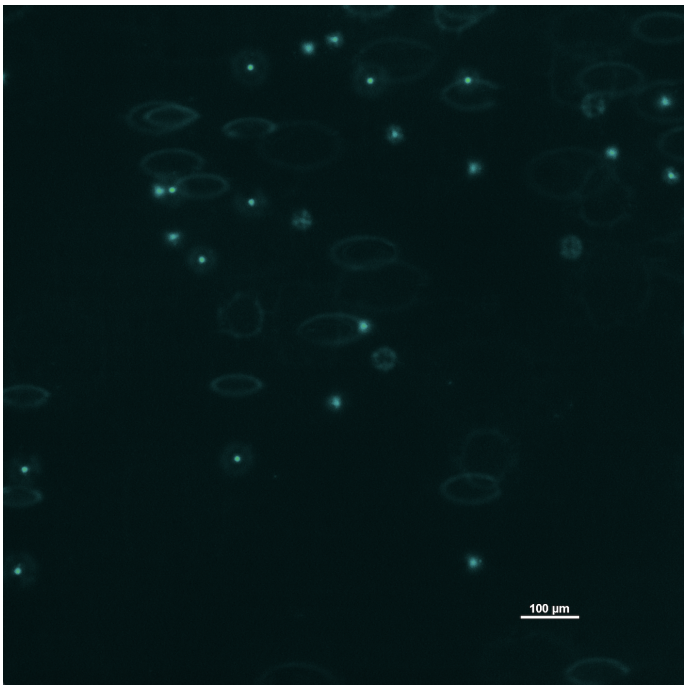


Figure 4.17: No clear patterns are found during the first two actuation experiments.

The second experiment was done exactly same as the first but with device 2. It was not showing any pattern during the actuation. However, this experiment was also intended to figure out the profile of velocity versus frequency. It can be determined that beads are near to or on the surface by observing their clear edge. The device was actuated with frequency

from 365 MHz to 390 MHz and power level of 5 dBm. Beads are moving with different velocities driven under different frequencies. Based on known results from Figure 4.18, the maximum velocity is approximately 6.27 $\mu m/s$ while they were actuating with frequency of 378 MHz. In addition, $S_{21}$ parameter plot showed that transmission power reached the maximum at the resonance frequency, which reflected in the velocity profile is that beads had maximum velocity at the resonance frequency.

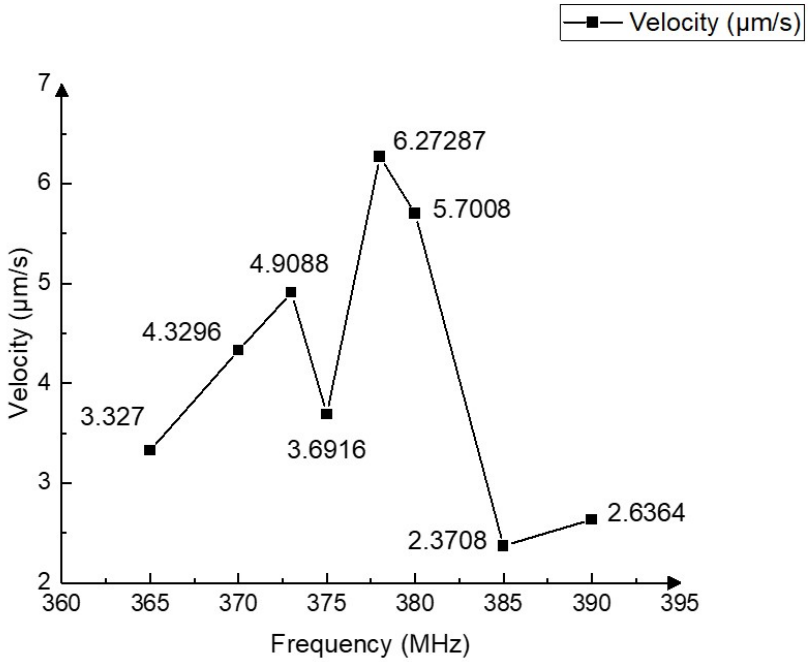


Figure 4.18: Velocities of micro-beads were measured during the second experiment of actuation. The highest velocity occurred when the device was actuated by 380 MHz acoustic wave.

In the third experiment, device 2 was used to actuate fluorescence beads. It was found that there are some patterns as shown in Figure 4.20a before actuating. Since it was not directly observed by microscope, there are several possible reasons. First, since the captured white light field image (Figure 4.20b) only showed part of the cavities matrix (Entire matrix is 40 x 40), trapping could happen in another part of the matrix. Another reason could be small amount of fluorescence beads got trapped during the cleaning procedure after first actuation. In experiments, the trapped beads still stuck in those cavities. Meanwhile, there were no additional beads getting trapped.

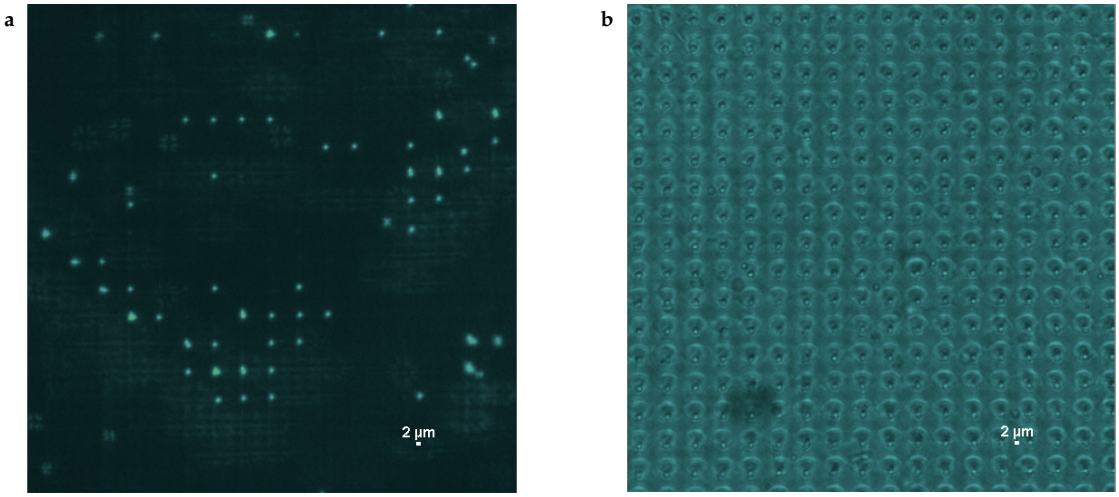


Figure 4.19: a) Patterns showed up before the third actuation which is observed through fluorescence microscope with 470 nm wavelength filter. b) White light image of the same area as the fluorescence image.

# 5 Discussion

Several challenges were found during fabrication and measurement of the device. It was found that top surface of the device was hydrophobic, which prevented the spin-coated material from forming a uniform layer. As shown in Figure 5.1, instead of becoming a thin film after spin coating, the NOA material remains as a droplet on the surface, making subsequent steps more challenging. To solve it, we tried to use oxygen plasma treatment to treat surface before spin coating the layer. By treating the surface for about 5 mins, it become hydrophilic at the end, and the film was generated. However, viewing the film under the microscope, it was easy to find that thickness of the film was not uniform. The film in the middle part is thicker than the film on the edge. The consequence of having un-uniform thickness film is creating more challenges to make the laser focus on the surface. This phenomenon is evidenced by Figure 4.17b.

Besides that, it was also found that those cavities were too far away from the substrate because the middle part of the layer is too thick. It can be the consequence of having relatively small area to spin coat. However, surface acoustic wave as an important tool of actuating beads concentrated most of power on the substrate surface. If the cavities are too far from the top surface of substrate, the surface acoustic wave is not powerful enough to trap the fluorescence beads. This can be the reason why the beads are not trapped during actuation. For the future work, the spin coating area in the middle of the substrate could be further increased to optimize the thickness uniformity.

Another phenomenon needs to be deeply considered. After turning on the function generator, the device was not actuated even though it was tested during S parameter measurement. After several round test, it was found that solution covered IDTs can short circuit and disable the actuation. However, considering the small area of the cavities matrix, it is hard to precisely put beads droplet in between each set of IDTs. In order to avoid the uncertainty of shorting circuit, a 320 $nm$ thick SiO2 layer was deposited on the substrate and directly covered IDTS with bound pad exposed.

With these challenges being solved, it is a method to fabricate the device which can precisely manipulate and trap the micron objects. It massively saved the time to fabricate a such device by using femtosecond laser. Meanwhile, it is a reliable device to deliver the micron objects for the future single molecule sequencing.

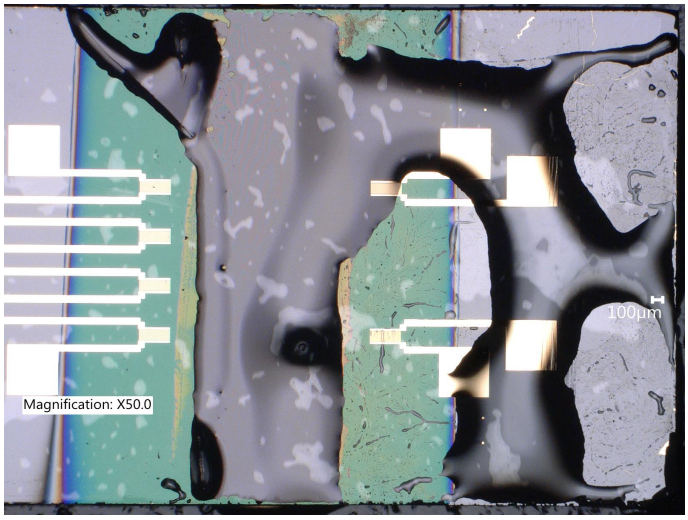


Figure 5.1: Since the top surface of the device is hydrophobic, NOA material falls apart after spin coating. The purple area is where the lithium niobate is located. The green area is 320 nm thick $SiO_2$*layer*.

# 6 Recommendations

While we did not directly observe the trapping of the fluorescence beads during actuation. However, some of the challenges have been discussed before. This chapter gives few suggestions for the future experiment, we can identify some challenges that were encountered and possible solutions to overcome them.

- For the layout of the device: Enlarge the middle area of the spin-coating cavity layer for better maneuverability
- Test the hydrophobicity of the device before spin coating any layers, and find out the possible reasons that could turn the surface into hydrophobic.
- Check the uniformity of thickness for the NOA layer, which is a prerequisite for successfully laser cutting cavities.
- Before laser cutting, ensure that the surface is in focus. Because it is difficult to tell if a surface is in focus by just looking at the diffraction fringes.
- During the actuation experiments, always keep checking on the droplet in order to avoid it drying out on the device. Residual beads from previous experiments will affect subsequent observations.

# 7 Conclusion

This thesis demonstrate the viability of a micron objects trapping device actuated by surface acoustic waves. The whole device consists of IDTs which generate surface acoustic wave and cavity layer which can trap the fluorescence beads. The goal of this research is to massively transport the sub-micron objects. By using surface acoustic waves coupled with a cavity array layer, these sub-micron objects can be non-invasively manipulated and hence brought closer to the sequencing areas(i.e. the nanopore in the chip). The achievements done by this research can greatly improve efficiency and reduce the cost of single molecules sequencing.

In this research, based on existed design of surface acoustic wave device, it was necessary to fabricate cavity layer onto the SAW device substrate. Two methods of fabricating cavity layer discussed in chapter 4.2. Through the comparison between two methods, femtosecond second laser is a more suitable way considering that cavity layer fabricated by that did not self-fluorescent. To fabricate a cavity layer, covering the IDTs with gel film during NOA material spin coating was implemented to prevent the NOA layer from covering the IDTs. The spin coated layer is cured under the exposure of UV light. After that, cavities were laser cut onto the NOA layer. By testing different parameters combination, we successfully fabricated cavity array layers and optimized dimension of cavities. Simulations of S parameters and acoustic pressure distribution were done in parallel. Simulation results were used as references to optimize experimental data.

Following the fabrication and optimization steps, we started to characterize the device by actuating it and manipulating fluorescence beads. The main goal of this research was to develop the platform which can manipulate sub-micron objects in-plane and trap them. In the fist two experiments, it was not found that any fluorescence beads trapped during actuation, nor after actuation. However, it was still clear to observe motion of the beads manipulated by surface acoustic wave. Meanwhile, the velocity profile of beads manipulated by different frequencies was extracted from captured videos. In the last experiment, it was found that beads were patterned in between actuation experiments. Through the analysis, the possible reasons can be summarized as trapping happened during second experiment which did not observed by the microscope or it happened during the cleaning procedure.

With application of Femtosecond laser, it is able to rapidly fabricate saw device with 2 $\mu m$ thick cavities array layer, which provides a feasible solution for manipulating sub-micron objects. However, there are several problems need to solved in the further experiments.

The idea of spin coating thin layer on top of dummy chip can be perfectly implemented. However, the thickness uniformity of spin-coated thin layers in a small area still challenges the feasibility of laser cutting the cavity. In order to achieve the sub-micron objects trapping, both thickness of the layer and depth of cavities are need to be more accurately control. In the final section we provided some practical recommendations that can help improve further work on this topic.

# Bibliography


[1] Laura L. Thompson, Brent J. Guppy, Laryssa Sawchuk, James R. Davie, and Kirk J. McManus. Regulation of chromatin structure via histone post-translational modification and the link to carcinogenesis. *Cancer and Metastasis Reviews*, 32:363–376, 12 2013.

[2] Anne C. Conibear. Deciphering protein post-translational modifications using chemical biology tools, 12 2020.

[3] Oxford Nanopore Technologies. Covid-19, 2022. [Online; 18- Mar- 2022].

[4] Helen Miller, Zhaokun Zhou, Jack Shepherd, Adam J M Wollman, and Mark C Leake. Single-molecule techniques in biophysics: a review of the progress in methods and applications. *Reports on Progress in Physics*, 81(2):024601, dec 2017.

[5] Daniel Johnson, Lu Bai, Benjamin Smith, Smita Patel, and Michelle Wang. Single-molecule studies reveal dynamics of dna unwinding by the ring-shaped t7 helicase. *Cell*, 129:1299–309, 07 2007.

[6] Adem Ozcelik, Joseph Rufo, Feng Guo, Yuyang Gu, Peng Li, James Lata, and Tony Jun Huang. Acoustic tweezers for the life sciences, 12 2018.

[7] Xiaoyun Ding, Peng Li, Sz Chin Steven Lin, Zackary S. Stratton, Nitesh Nama, Feng Guo, Daniel Slotcavage, Xiaole Mao, Jinjie Shi, Francesco Costanzo, and Tony Jun Huang. Surface acoustic wave microfluidics, 9 2013.

[8] Jorge Puebla, Mingran Xu, Bivas Rana, Kei Yamamoto, Sadamichi Maekawa, and Yoshichika Otani. Acoustic ferromagnetic resonance and spin pumping induced by surface acoustic waves. *Journal of Physics D: Applied Physics*, 53(26):264002, may 2020.

[9] Kamsma D. Thalhammer G. et al. Sitters, G. Acoustic force spectroscopy. *Nature*, pages 47–50, 11 2014.

[10] David J. Collins, Belinda Morahan, Jose Garcia-Bustos, Christian Doerig, Magdalena Plebanski, and Adrian Neild. Two-dimensional single-cell patterning with one cell per well driven by surface acoustic waves. *Nature Communications*, 6, 11 2015.

[11] Mahnoush Tayebi, Richard O'Rorke, Him Cheng Wong, Hong Yee Low, Jongyoon Han, David J. Collins, and Ye Ai. Massively multiplexed submicron particle patterning in acoustically driven oscillating nanocavities. *Small*, 16, 4 2020.

[12] Lithium niobate crystals.

[13] NT-MDT spectrum instruments. https://www.ntmdtsi.com/resources/spm-theory/theoretical- background- of- spm/2- scanningforce - microscopy - (sfm ) /22 - cantilever - sample - force - interaction / 221 - cantilever-sample-interaction-potential-afm-operation-modes., 04 2022.

[14] What is afm? learn about atomic force microscopy! - nanoandmore. *Nanoandmore.com*, 2022.

[15] Ch. Gerber G. Binnig, C. F. Quate. Atomic force microscope. *Phys. Rev. Lett. 56*, pages 930–933, 1986.

[16] Rahman Sabahi-Kaviani and Regina Luttge. Investigating the pattern transfer fidelity of norland optical adhesive 81 for nanogrooves by microtransfer molding. *Journal of Vacuum Science & Technology B*, 39(6):062810, 2021.

[17] W. Sibbett, A. A. Lagatsky, and C. T. A. Brown. The development and application of femtosecond laser systems. *Opt. Express*, 20(7):6989–7001, Mar 2012.

[18] Ada-Ioana Bunea, Nuria del Castillo Iniesta, Ariadni Droumpali, Alexandre Emmanuel Wetzel, Einstom Engay, and Rafael Taboryski. Micro 3d printing by two-photon polymerization: Configurations and parameters for the nanoscribe system. *Micro*, 1:164–180, 9 2021.

[19] Joachim Fischer and Martin Wegener. Three-dimensional optical laser lithography beyond the diffraction limit. *Laser & Photonics Reviews*, 7(1):22–44, 2013.

[20] T.; Takada K. Kawata S.; Sun, H.B.; Tanaka. Finer feature for functional microdevices. *Nature*, pages 697–698, 2001.

[21] Gift Nyikayaramba and Boris Murmann. S-parameter-based defect localization for ultrasonic guided wave shm. *Aerospace*, 7:33, 03 2020.

[22] Gift Nyikayaramba and Boris Murmann. S-parameter-based defect localization for ultrasonic guided wave shm. *Aerospace*, 7:33, 03 2020.

[23] JA. Lichtman, J.; Conchello. Fluorescence microscopy. *Nat Methods*, 2005.

[24] Teledyne Photometrics. What do you know about fluorescence? 2020.

[25] A low-autofluorescence, transparent resin for multiphoton 3d printing.

[26] A Einstein. The motion of elements suspended in static liquids as claimed in the molecular kinetic theory of heat, 1905.